Crustal and upper mantle structure of northern Tibet imaged with magnetotelluric data

Martyn Unsworth,[1] Wei Wenbo,[2] Alan G. Jones,[3] Shenghui Li,[4] Paul Bedrosian,[4] John Booker,[4] Jin Sheng,[2] Deng Ming,[2] and Tan Handong[2]

Received 13 November 2002; revised 14 October 2003; accepted 21 November 2003; published 13 February 2004.

[1] Magnetotelluric (MT) data were collected in northern Tibet along the Amdo to Golmud highway during the 1995 and 1999 Project INDEPTH (International Deep Profiling of Tibet and the Himalaya) surveys. Broadband and long period MT data were collected and the TE-mode, TM-mode and vertical magnetic field data were inverted to yield a minimum structure, two-dimensional resistivity model. The model obtained from inverting all responses simultaneously shows that a pervasive midcrustal conductor extends from the Kunlun Shan to the Bangong-Nuijiang suture. The vertically integrated conductivity (conductance) of this crustal layer is greatest in the northern Qiangtang terrane at latitude 34°N. The electrical resistivity of the upper mantle is constrained by the MT data to be in the range of 10–30 Ωm across the Songpan-Ganze and Qiangtang terranes. This is lower than would be expected if Asian lithosphere underthrusts northern Tibet as far as the Qiangtang terrane. The MT responses are more consistent with a model in which Asian lithosphere extends as far south as the Kunlun Shan, and the upper mantle beneath the Songpan-Ganze and Qiangtang terranes is sufficiently hot to contain a small fraction of interconnected partial melt. *INDEX TERMS:* 8102 Tectonophysics: Continental contractional orogenic belts; 7205 Seismology: Continental crust (1242); 1515 Geomagnetism and Paleomagnetism: Geomagnetic induction; 8123 Tectonophysics: Dynamics, seismotectonics; *KEYWORDS:* Tibetan Plateau, Kunlun Fault, magnetotellurics, Qiangtang terrane

Citation: Unsworth, M., W. Wei, A. G. Jones, S. Li, P. Bedrosian, J. Booker, S. Jin, M. Deng, and H. Tan (2004), Crustal and upper mantle structure of northern Tibet imaged with magnetotelluric data, *J. Geophys. Res.*, *109*, B02403, doi:10.1029/2002JB002305.

1. Introduction

[2] The Tibetan Plateau is the direct result of the ongoing collision between India and Asia that began with the closure of the Tethys Ocean in the Eocene. A wide range of geodynamic models have been proposed for the evolution of the Tibetan Plateau and include the spectrum from whole scale underthrusting of Indian or Asian lithosphere [*Argand*, 1924; *Ni and Barazangi*, 1983; *Willett and Beaumont*, 1994; *Tapponnier et al.*, 2001] to distributed shortening [*Dewey and Burke*, 1973]. Only in the last decade have geological and geophysical studies been undertaken that can differentiate between these competing hypotheses for the structure and evolution of the Tibetan Plateau. While many early studies were located in the Himalaya and southern Tibet [*Zhao et al.*, 1993; *Nelson et al.*, 1996; *Hirn et al.*, 1997] it has become clear that a complete understanding of the structure and evolution of the Tibetan Plateau requires a study of the entire plateau. This is especially true of northern Tibet, where the plateau continues to grow to the northeast [*Tapponnier et al.*, 2001]. Very different geodynamic processes have been proposed for the formation of the crustal and mantle structures observed today in northern Tibet. In one interpretation, Asian lithosphere is being subducted beneath the northern margin of the Tibetan Plateau [*Tapponnier et al.*, 2001, and references therein]. Alternatively, this boundary is simply characterized by a change in crustal thickness, with northern Tibet supported by a hot upper mantle [*Owens and Zandt*, 1997; *Zhu and Helmberger*, 1998]. Similar uncertainty surrounds the processes that are active in the upper mantle beneath the Qiangtang and Songpan-Ganze terranes of northern Tibet (Figure 1). Plio-Pleistocene volcanic rocks are widely distributed in northern Tibet and their origin is disputed [*Turner et al.*, 1993; *Arnaud et al.*, 1992]. One explanation is that lithospheric delamination occurred when thickened lithosphere became mechanically unstable resulting in localized convection of the asthenosphere [*Molnar*, 1988; *England and Houseman*, 1989]. Seismic evidence for a hot upper mantle that does not transmit shear waves was taken to support this hypothesis [*Owens and Zandt*, 1997]. Alternatively, the volcanic rocks might

[1]Institute for Geophysical Research and Department of Physics, University of Alberta, Edmonton, Canada.
[2]Department of Applied Geophysics, China University of Geoscience, Beijing, China.
[3]Geological Survey of Canada, Ottawa, Canada.
[4]Department of Earth and Space Sciences, University of Washington, Seattle, USA.

0148-0227/04/2002JB002305$09.00

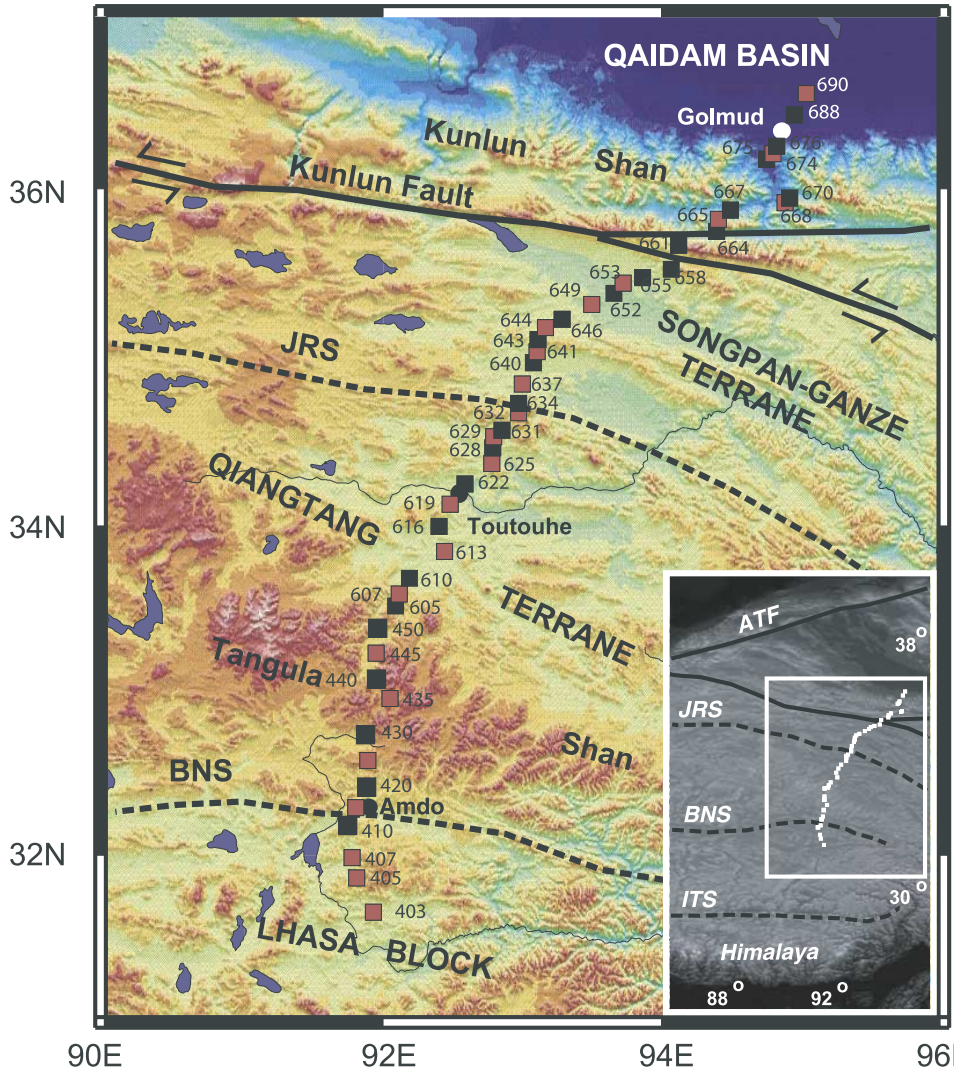

Figure 1. Location of the 600-line MT transect that follows the Golmud-Amdo highway. The black squares show locations where both broadband and long period MT data were collected. At the other locations (red squares), only broadband MT data were collected. Abbreviations are as follows: BNS, Banggong-Nuijiang Suture; JRS, Jinsha River Suture; ITS, Indus Tsangpo Suture; ATF, Altyn Tagh fault.

reflect episodes of the subduction of Asian lithosphere stepping to the north [*Tapponnier et al.*, 2001].

[3] In this paper the previous geological and geophysical studies of northern Tibet are reviewed, and the analysis and interpretation of magnetotelluric (MT) data acquired in northern Tibet is described. The paper is focused on regional-scale geoelectric structure and concludes with possible models to account for the field observations.

2. Previous Geophysical and Geological Studies in Northern Tibet

2.1. Regional Geology

[4] The geology of central and northern Tibet is characterized by a series of allochthonous terranes that were accreted to the southern margin of Asia prior to the arrival of the Indian continent [*Dewey et al.*, 1988]. The suture zones bounding these terranes may have been reactivated by the deformation resulting from the India-Asia collision to the south [*Tapponnier et al.*, 2001, and references therein]. The northern limit of the MT profile described in this paper (the 600-line) is located in the landlocked Qaidam Basin (Figure 1) whose infilling has resulted in a sedimentary sequence at least 5 km thick [*Chen et al.*, 1999; *Metevier et al.*, 1998]. To the south lies the Kunlun Shan, a Paleozoic-Triassic collisional belt characterized by a series of granitic plutons that intruded Ordovician-Permian sedimentary rocks [*Coward et al.*, 1988; *Mock et al.*, 1999]. The Paleozoic Anyimaqen-Kunlun-Muztagh suture defines the southern edge of the Kunlun Shan in the study area [*Dewey et al.*, 1988; *Yin and Harrison*, 2000, and references therein]. Structures in the Kunlun Shan were apparently reactivated by the India-Asia collision [*Tapponnier et al.*, 2001], and have involved both uplift on thrust faults [*Mock et al.*, 1999] and the development of the Kunlun fault, a major left-lateral strike slip fault system [*Kidd and Molnar*, 1988; *Lin et al.*, 2002]. Estimates of the total right lateral offset on the Kunlun fault range from 75 km to 500 km

[*Kidd and Molnar*, 1988; *Matte et al.*, 1996]. The Kunlun fault splays into two branches at the location of the MT profile (the trace of the highway is marked by the MT stations in Figure 1). Paleoseismological studies on the northern (Xidatan) segment indicate an average slip rate of 12 mm per year over the last 100,000 years [*van der Woerd et al.*, 1998]. Together with active thrusting in the Kunlun Shan, these strike-slip faults permit both north-south convergence and the eastward escape of the lithosphere to the south of the Kunlun fault.

[5] The Songpan-Ganze terrane lies between the Kunlun Shan and Triassic Jinsha suture. In this terrane a thick Triassic flysch complex deposited on Paleozoic shelf units dominates the surface geology. To the south lies the Qiangtang terrane, which is bounded by the Jinsha River and Bangong-Nuijiang sutures on the north and south respectively. The Qiangtang terrane was accreted to Asia in the Late Triassic or Early Jurassic. Along the route of the Lhasa-Golmud highway the surface geology of the Qiangtang is predominantly Jurassic in age and comprises a mixture of sedimentary units with extensive granitic intrusions in the Tangula Shan. Further west the geology of the Qiangtang terrane is more varied, with extensive zones of metamorphic rocks and late Paleozoic to Jurassic sedimentary rocks [*Kapp et al.*, 2000; *Yin and Harrison*, 2000]. Significant Plio-Pleistocene volcanism has occurred in both the Songpan-Ganze and northern Qiantang terranes. The petrology of these volcanic rocks suggests that they originated by melting of subcontinental lithospheric mantle, with the presence of a significant crustal component [*Turner et al.*, 1993; *Arnaud et al.*, 1992; *Tapponnier et al.*, 2001, and references therein]. Some of these volcanic rocks are clustered along the active strands of the Kunlun and Altyn Tagh faults. *Molnar* [1988] proposed that these volcanic rocks were the product of delamination of a zone of thickened lithosphere that resulted in localized upwelling of the asthenosphere. However, other studies question whether the mantle rocks originated in asthenospheric or mantle plume sources, and instead proposed that they originate in crustal melting that occurred as Asian lithosphere subducts southward beneath northern Tibet [*Tapponnier et al.*, 2001]. Those same authors also suggest that the present location of volcanism is merely the latest in a sequence of north-migrating subduction events. In a modified subduction scenario, *Kapp et al.* [2000] proposed the southward directed subduction of the Songpan-Ganze flysch complex at the Jinsha River suture injected water into the lower crust and initiated widespread crustal melting that led to the late Cenozoic volcanism in northern Tibet.

2.2. Seismic Exploration in Northern Tibet

[6] The 1992-3 PASSCAL survey deployed broadband seismic stations across the complete north-south extent of the Tibetan Plateau for the first time [*Owens and Zandt*, 1997]. Travel time tomography and receiver function analysis showed that there are first order differences in seismic structure between northern and southern Tibet. In southern Tibet the crust is 80 km thick and underlain by a relatively fast (cold) upper mantle. A thinner crust was inferred in northern Tibet with anomalously high values of Poisson's ratio in the Songpan-Ganze and northern Qiangtang terranes [*Owens and Zandt*, 1997]. The crust was found to be thinnest in the Songpan-Ganze terrane. The PASSCAL survey also showed that shear waves do not propagate efficiently in the upper mantle in northern Tibet, implying high temperatures and possibly partial melting. The zone of shear wave attenuation in the upper mantle is spatially coincident with the distribution of Plio-Pleistocene volcanic rocks in northern Tibet and the location where upwelling asthenosphere is predicted by models requiring delamination as a response to crustal thickening [*Molnar*, 1988; *England and Houseman*, 1989]. More recent surface wave studies have confirmed these first order differences in upper mantle structure between northern and southern Tibet [*Rapine et al.*, 2003]. Recent receiver function studies also confirm that the upper mantle is hotter beneath northern Tibet, compared to southern Tibet [*Kind et al.*, 2002]. However, receiver function analysis of the PASSCAL data using other seismic phases showed that other velocity models could fit the data equally well, with the anomalous crustal structure confined to the lower part of a thicker crust or even with the Poisson's ratio close to the average value for the continents [*Vergne et al.*, 2002]. Receiver functions analysis suggest that there is a 10 km step in the Moho beneath the northern boundary of the Kunlun Shan, with a thinner crust to the north [*Zhu and Helmberger*, 1998].

[7] An alternative view of lithospheric structure beneath northern Tibet is summarized by *Tapponnier et al.* [2001], who proposed that subduction of Asian lithosphere, combined with major strike-slip faulting, has led to the rise of the northern Tibetan Plateau. Despite the results of the PASSCAL seismic experiment, these investigators have focused on surface wave data that suggest high average velocities from the surface to a depth of 200 km beneath Tibet [*Griot et al.*, 1998]. Combined with geological studies, they suggested that Asian lithosphere is being subducted to the south, leading to widespread melting. Geodynamic modeling has demonstrated that the observed location of suture zones and regional geology is indeed consistent with southward subduction of Asian lithosphere [*Willett and Beaumont*, 1994], but seismic evidence for subducting Asian lithosphere beneath northern Tibet is ambiguous. *Wittlinger et al.* [1996] used teleseismic signals to image a block structure in the crust and give evidence for low velocities in the upper mantle in the depth range 200–300 km beneath the northern Qiangtang and Songpan-Ganze terranes. These low velocities could result from partial melting in the upper mantle, as would be expected by both the continental subduction and upwelling asthenosphere hypotheses. However, the depth is greater than expected for both of these phenomena, and might reflect the inadequate resolution of the analysis technique used. The most recent deep seismic results from northern Tibet are the combined receiver function analyses derived from a compilation of all available data [*Kosarev et al.*, 1999; *Kind et al.*, 2002]. These studies reveal a south dipping converter that is interpreted as being Asian Lithospheric Mantle, and which gives support for the subduction of Asian lithosphere beneath northern Tibet. These receiver function analyses also show less north-south variation in crustal thickness than previously reported [*Owens and Zandt*, 1997]. *Galve et al.* [2002] present seismic refraction data using explosive sources from northeastern Tibet that revealed a crust thickened by successive thrust faulting and stacking, but with no

evidence of partial melting to the north of the Jinsha River suture.

2.3. Magnetotelluric Exploration of Tibet

[8] Additional information about the structure, fluid content and rheology of the lithosphere can be derived by remotely sensing the electrical conductivity of the Earth. For exploration of electrical structure to depths beyond 10 km, the only viable technique is magnetotellurics (MT), which uses natural electromagnetic waves as an energy source. The first magnetotelluric data collected in Tibet were acquired during the Sino-French collaboration in the 1980s and revealed that the crust in southern Tibet was unusually conductive [*van Ngoc et al.*, 1986]. This high conductivity was attributed to partial melting in the crust. Broadband MT data were also collected by the China University of Geoscience (Wuhan) in central Tibet [*Shengye et al.*, 1996] and gave additional evidence for high crustal conductivity. A combination of broadband and long-period MT data (capable of imaging deeper structure) was first collected in Tibet during the INDEPTH project in 1995. This study produced more detailed images of crustal resistivity and further evidence that widespread fluids, probably partial melt, were present in the mid crust of southern Tibet [*Chen et al.*, 1996]. To understand the orogenic processes at work in northern Tibet, the INDEPTH MT survey was extended in 1999 along the Amdo-Golmud highway to the Qaidam Basin. An initial interpretation of these MT data showed that the conductive crust found in southern Tibet is also present in northern Tibet [*Wei et al.*, 2001]. In this paper a more detailed analysis of the MT data is presented, and the significance of the results is evaluated.

3. The 600-Line Magnetotelluric Data

3.1. MT Data Collection and Processing

[9] Long period MT data were collected in 1995 at five locations in the southern Qingtang terrane. The 1999 data comprised long period MT data at 25 locations and broadband MT data (100 Hz–10,000 s) at 41 locations (Figure 1). The long period MT data were collected with the LIMS instruments developed by the Geological Survey of Canada, based on ring core fluxgate magnetometers [*Narod and Bennest*, 1990]. The broadband MT data were acquired with two Electromagnetic Instruments Incorporated (EMI) MT-24 systems. The time series data were processed to yield estimates of impedance as a function of period, using remote reference data when available [*Egbert*, 1997; *Jones et al.*, 1989]. The long period and broadband MT data were then merged into single responses for each station, after allowing for the differences in electrode array layout. Where necessary, the apparent resistivity curves of the long-period MT data were shifted to the level of the broadband data. This shift was generally small, typically less than 20% of the apparent resistivity.

3.2. Tensor Decomposition and Geoelectric Strike Analysis

[10] Before magnetotelluric data can be used to derive resistivity models of subsurface structure, the dimensionality and directionality of the data must be evaluated. The most effective way of doing this is using tensor decomposition, which determines if a two-dimensional (2-D) or 3-D approach is most appropriate. In the case of a 2-D scenario, it gives an estimate of the geoelectric strike direction. The 600-line data were analyzed using the multisite, multifrequency, tensor decomposition algorithm of *McNeice and Jones* [2001], which is based on the method of *Groom and Bailey* [1989]. Most sites were relatively undistorted with twist and shear angles less than 10°. These angles measure the degree of electric field distortion, with highly distorted sites exhibiting values of 60° and 45° respectively. A number of stations in the Kunlun Shan showed significant distortion with shear angles in excess of 30° (a shear angle of 45° indicates that there is severe electric field distortion at the site resulting in a singular impedance tensor). This is due to the locations of these stations in deep valleys on thin strips of conductive sediments, which results in the electric fields being completely polarized along the valleys. With the exception of the distorted sites in the Kunlun Shan, the galvanic distortion model gave a good fit to the observed MT impedance responses. The results of single site tensor decomposition are summarized in Figure 2, which shows the best fitting geoelectric strike for both the entire period band, and also individual, decade-wide, bands. Note that there is an inherent ambiguity of 90° in the strike angle determined with tensor decomposition. Allowing for this ambiguity, Figure 2 shows that a strike direction in the range east to E20°S is the most appropriate for these data (or orthogonal directions).

[11] Multisite, multifrequency, tensor decomposition was also applied to the MT data and the results are summarized in Figure 3. This shows the best fitting geoelectric strike direction for all 46 sites for period bands one decade wide. Note that the decomposition fits the measured data with statistically acceptable misfits at most sites. The strike direction yielding the lowest global misfit lies between N10°E and N30°E (or E10°S to E30°S), consistent with the site-by-site strike analysis. To resolve the 90° ambiguity in strike determination, external information is required to distinguish between the two possible, orthogonal directions. In northern Tibet the surface strike of major terrane boundaries indicates that E20°S is much more reasonable than N20°E. This choice of strike direction is also confirmed by the magnetic induction vectors described below. Thus, a strike direction of E20°S was chosen for subsequent modeling and inversion of the 600-line MT data, consistent with the surface expression of the major geological features shown in Figure 1.

3.3. Magnetotelluric Pseudosections

[12] The magnetotelluric data in the E20°S coordinate frame are displayed in pseudosection format in Figure 4. Plotting the MT data with period on the vertical axis and distance on the horizontal axis gives a qualitative impression of resistivity variations with depth and distance along the profile. The horizontal scale is distance from the most northern station in the Qaidam Basin (station TBT690 in Figure 1). The apparent resistivity observed for both electric field aligned parallel to strike (Tangential Electric, or TE, mode of induction) and perpendicular to strike (Tangential Magnetic, or TM, mode of induction) varies as expected for the shallow geology along the profile:

[13] 1. Low apparent resistivities (<10 Ωm) and high phases are observed in the Qaidam Basin at the two

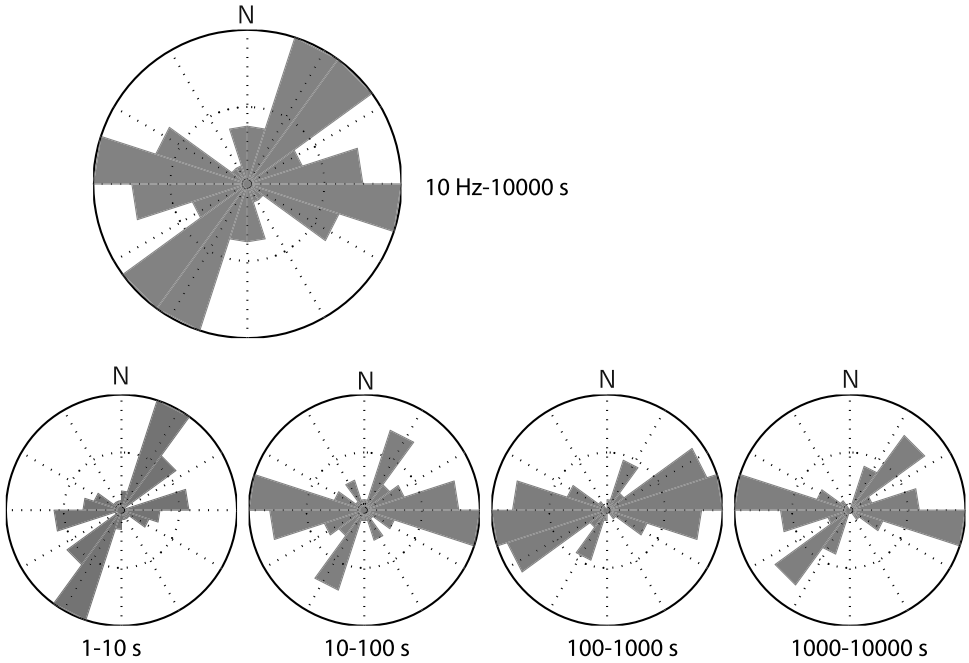

Figure 2. Single site tensor decomposition of 600-line magnetotelluric data. The histograms show the distribution of geoelectric strike directions for decade wide period bands.

northernmost sites TBT688 and TBT690 due to the presence of Quaternary sediments (distances of 0–30 km).

[14] 2. High apparent resistivities (>100 Ωm) and low phases in the Kunlun Shan are observed due to resistive crystalline rocks (30–150 km).

[15] 3. Intermediate apparent resistivity (10–100 Ωm) and moderately high phase is observed across the sedimentary basins in the Songpan-Ganze terrane and also in northern Qiantang Terrane (150–400 km).

[16] 4. High apparent resistivity (>1000 Ωm) and moderately low phase is observed in the Tangula Shan of the southern Qiangtang terrane where crystalline rocks are exposed at the surface (400–600 km).

[17] The vertical stripes in the apparent resistivity pseudosections are partly due to site-to-site variations in shallow resistivity structure. These so-called static shifts are the result of shallow resistivity structures producing a change in the measured apparent resistivity at all periods [*Jones*, 1988]. This phenomenon does not affect the phase, and thus the phase pseudosections display a smoother spatial variation. The most conspicuous feature in the phase pseudosections is the high phases (>60°) in both modes at periods from 100 to 1000 s, from the Kunlun fault to the Banggong-Nuijiang suture. This high phase indicates the presence of a conductive crustal layer. Figure 5 shows the phase at three representative sites along the profile. Note that at the longest periods, φ_{TE} is less than 45°, indicating an increase in resistivity at depth. The φ_{TM} remains high at long period, and it will be shown that this is due to the effect of electric charges on the north and south edges of the conductor. The long period MT responses at sites in the Kunlun Shan and Qaidam Basin (0–100 km) are generally of low quality. This was due to a combination of distortion and the high conductivity of the near-surface structure in the Qaidam basin. This lack of coverage results in poor constraint on the deep structure of the northern end of the profile. The vertical magnetic field data at these sites partially compensates for the lack of usable MT impedance data.

3.4. Vertical Magnetic Field Data

[18] Vertical magnetic field (H_z) data were also recorded in both 1995 and 1999. Above a one-dimensional Earth, the vertical magnetic field generated by plane wave MT source fields is zero. However, if the profile crosses a conductor, then electric currents flowing in the conductor will generate a vertical magnetic field with an upward component on one side of the conductor, and a downward component on the other. The geomagnetic transfer functions (TF) between the vertical magnetic field and the two horizontal magnetic field components are derived in a similar manner to MT imped-

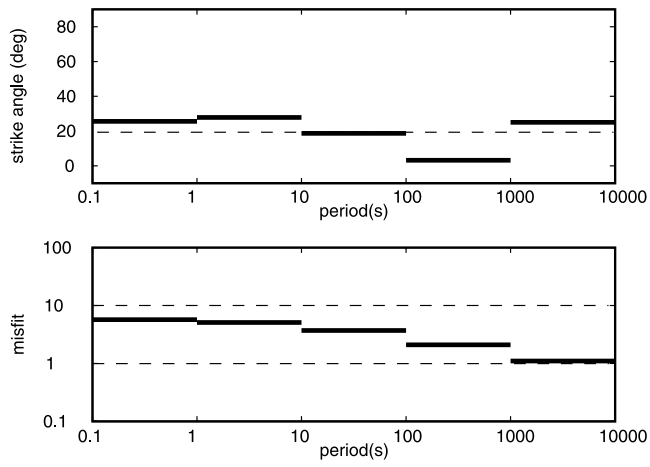

Figure 3. Multisite tensor decomposition of the 600-line MT data for decade wide period bands.

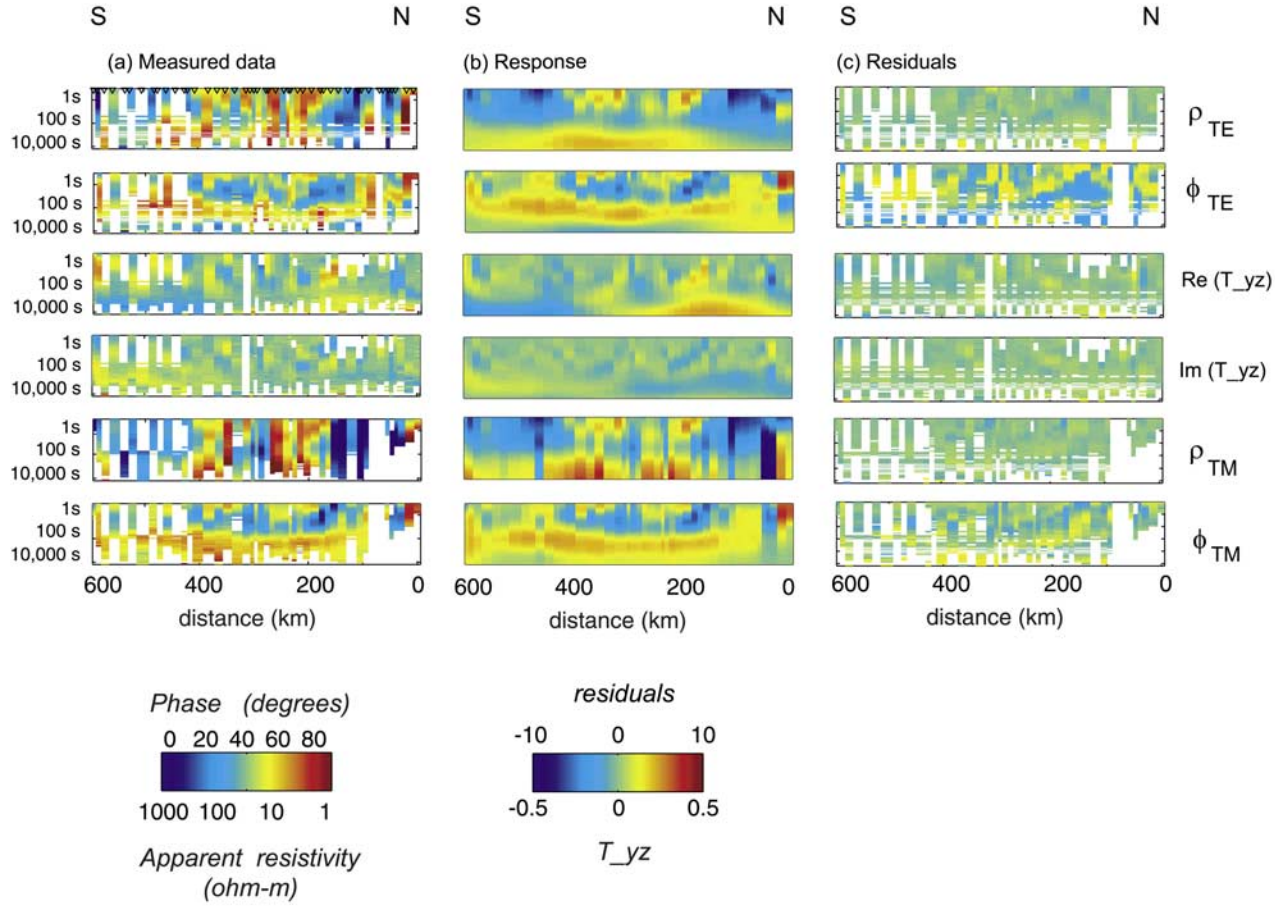

Figure 4. (a) Magnetotelluric data and vertical magnetic field transfer functions (dimensionless) in pseudosection format for the 600-line. (b) Response of the model in Figure 7. (c) Misfit in terms of residuals (standard errors). Data are shown in a N20°E coordinate system. White areas denote bad or missing data.

ance. These quantities are often plotted in map view as magnetic induction vectors with the length of the vector proportional to the magnitude of the vertical magnetic field [*Parkinson*, 1962]. In the convention used in this paper, the real, in-phase vector points at conductive structures. The vectors at a period of 3400 s generally point N20°E or S20°W, i.e., parallel to the profile, giving additional confirmation of the geoelectric strike direction derived from tensor decomposition (Figure 6). Note the reversal in the direction of the vectors at approximately 34°N, which indicates the location of a major conductive structure or boundary. The vertical magnetic field data can also be displayed as a pseudosection of the transfer function between the vertical component and the horizontal component parallel to the profile (T_{zy}), as shown in Figure 4. The reversal discussed above can be observed in the real T_{zy} pseudosection from periods of 1000–10,000 s, with values of +0.2 to the north and −0.2 to the south.

4. Forward Modeling and Inversion of MT and Vertical Magnetic Field Data

[19] The initial analysis of these data by *Wei et al.* [2001] used the TM-mode data alone, and revealed the widespread extent of the Tibetan crustal conductor (TCC). The TE-mode and T_{zy} data contain additional information and should be included in a full analysis. However, TE data can be more sensitive to 3-D effects, and should be used with care [*Wannamaker et al.*, 1984; *Ledo et al.*, 2002]. In this section, the simultaneous inversion of TM, TE and T_{zy} data is described. The resulting model is then justified by constrained inversions, synthetic inversions and 2-D and 3-D forward modeling.

4.1. Two-Dimensional Inversion of TE, TM and T_{zy} Data

[20] The inversion algorithm of *Rodi and Mackie* [2001] was used to determine the range of resistivity models consistent with the 600-line MT data. The TM, TE and T_{zy} data were inverted individually and together. A range of error floors were investigated and used to determine the degree of mutual consistency between the various components of the data. Figure 7 shows the model derived by inverting all the data from a 100 Ωm half-space starting model and represents a compromise between fitting the TE, TM and T_{zy} data. This model was derived after 125 iterations, and has an overall root-mean-square (RMS) misfit of 1.63. This number of iterations may seem large,

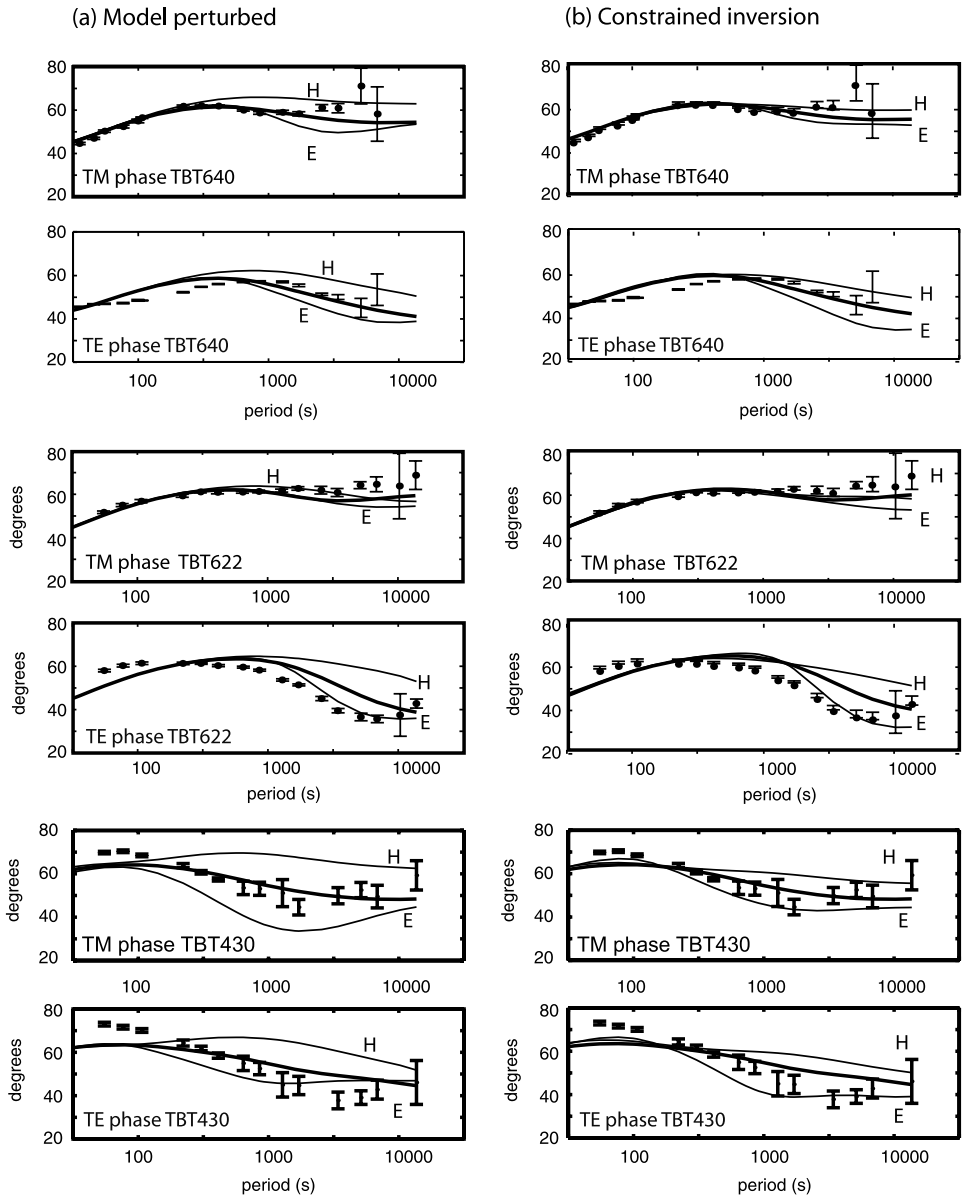

Figure 5. (a) MT phase responses at three typical stations on the 600-line. Site 21 (Songpan-Ganze terrane), site 29 (northern Qiangtang terrane), and site 40 (southern Qiangtang terrane). The thick central curve is the response of the best fitting model shown in Figure 7. The upper curve (H) is the predicted response of model with a uniform 3 Ωm layer extending from the midcrustal layer to 200 km. The lower curve (E) is for a 100 Ωm layer extending to 200 km. (b) Shows results of constrained inversions. The inversion was restarted from the perturbed models, with the perturbed region fixed.

but is typical for this inversion algorithm [*Rodi and Mackie*, 2001]. The inversion used error floors of 100% in TM apparent resistivity, 200% in TE apparent resistivity and 2.86° (5%) in TM and TE phase. An error floor of 0.05 was used in T_{zy}. The fit to the measured data is shown in Figure 4. The RMS misfit of the model to the measured MT data for each site is shown as a function of station number in Figure 8 and is reasonably uniform. The fit is also shown for three typical MT sites and it can be seen that the data are generally well fit at long periods (Figure 5). However, some inconsistencies between the TE mode and TM mode fits can be observed. For example, at site TBT622, the inversion predicts TM phases that are too low, while the predicted TE phase is too high. This is probably due to minor 3-D effects in the data that impose a limit on how closely the data can be fit with a 2-D inversion.

[21] Various strategies were used to evaluate the effects of static shifts on the model. These included allowing the inversion to estimate the static shift coefficients and also down weighting the apparent resistivities through the use of a large error floor as discussed above. Both procedures, with a range of parameters, resulted in similar

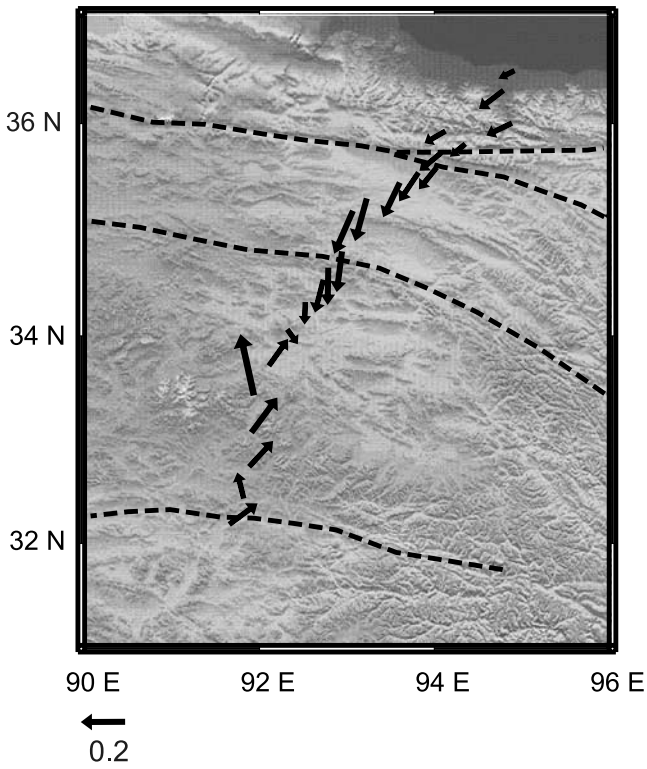

Figure 6. Real induction vectors at a period of 3400 s. Note that the arrows are approximately parallel to the profile giving additional support for the geoelectric strike derived from the tensor decomposition. The reversal near 34°N indicates the center of a major conductor.

resistivity models. The static shifts for the TE-TM-T_{zy} model are shown in Figure 9, and it can be seen that they scatter around a mean value that is close to one. Some static shift coefficients are large, but this method of estimation appears robust and is justified through the synthetic inversion study described below. The TE-TM-T_{zy} model is significantly less conductive than models derived with only the TM and T_{zy} data (not shown). The conductive layer is limited to the crust and does not extend into the upper mantle. The apparent extension of the conductive structure into the upper mantle is probably due to the smoothing imposed in the inversion procedure and to the inherent lack of sensitivity to structure directly below a conductor. In the following sections, the sensitivity of this model to the measured data will be examined.

4.2. Two-Dimensional Forward Modeling

[22] In order to understand the physical origin of the long period MT phase behavior, a simple 2-D geoelectric model was constructed. Two representative models and responses are illustrated in Figure 10. At stations above the Tibetan Crustal Conductor (TCC), the TE mode apparent resistivity (ρ_{TE}) levels out and rises at the longest periods as the EM signals sample the more resistive upper mantle. This results in values of φ_{TE} below 45°. In contrast, the TM mode apparent resistivity (ρ_{TM}) continues to decrease, even at 10,000 s. This is because electric charges on the vertical boundaries of the conductor weaken electric field within the conductor and at stations above it. The negative gradient of $d(\log \rho_{TM})dT$ gives the high values of φ_{TM} where T is the period of the signal. A range of forward models was evaluated in the study, and it was found that a conductor in the form of a single rectangular prism could not readily produce the observed split in φ_{TM} and φ_{TE} at long periods. The additional vertical edges at 260 km and 480 km are needed to produce the phase split. This model is similar to the inversion result in Figure 7 and gives a physical understanding to the origin of the primary features in the observed data.

4.3. Sensitivity of Middle and Lower Crustal and Upper Mantle Resistivity Model to the Measured MT Data

[23] The model in Figure 7 shows major variations in the resistivity structure in the middle to lower crust and upper mantle of northern Tibet. Before interpreting these differ-

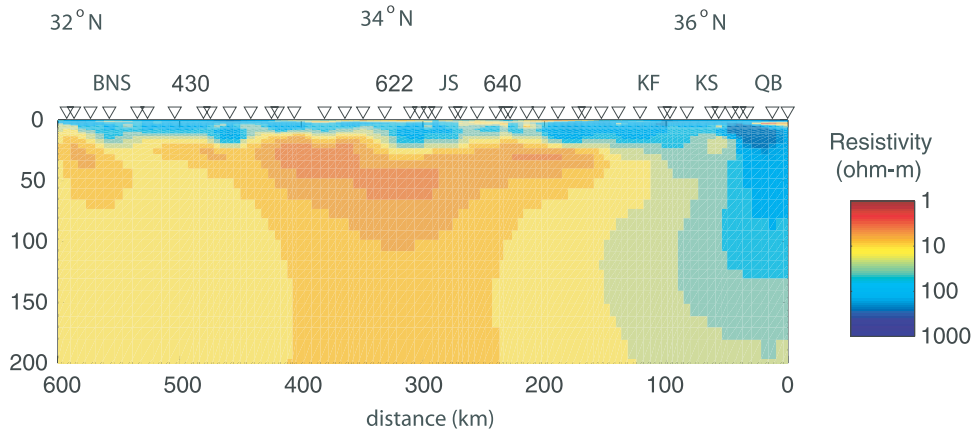

Figure 7. Resistivity model for the joint inversion of TE, TM and T_{zy} data 600-line data. Model shown with a 1:1 vertical exaggeration. (Model: temhz-33.) Abbreviations are as follows: BNS, Bangong-Nuijiang suture; JS, Jinsha Suture; KF, Kunlun fault; KS, Kunlun Shan; QB, Qaidam Basin.

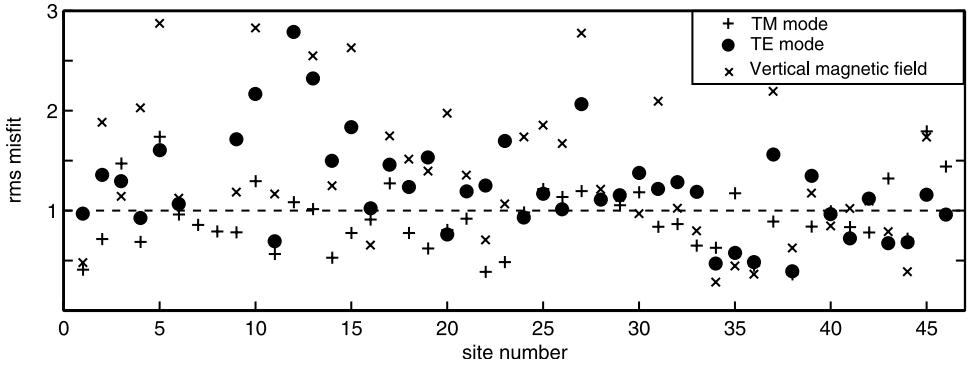

Figure 8. Site by site RMS misfit for the resistivity model shown in Figure 7.

ences, it is important to determine the degree to which they are required by the data. MT impedance data are most sensitive to the depth of a conductive layer, and to the total conductance of the layer, provided that the electromagnetic fields penetrate through the layer completely. If they do not, they provide a minimum value for the conductance. MT data are less sensitive to the individual thicknesses and conductivities that make up a given conductance. It should also be considered that MT cannot always resolve a conductor at depth if it is overlain by a shallower conductor. In the following section the data requirements for the four major zones will be considered.

4.3.1. Qaidam Basin and Kunlun Shan

[24] The lithosphere in this zone is relatively resistive (>100 Ωm) and underlain by lower resistivity below 100 km. This resistive structure is primarily required by the MT responses at the northern end of the profile. The T_{zy} responses also require high resistivity in this zone, compared to the lower values to the south. It is this north-south contrast in resistivity that contributes to the reversal in T_{zy} at long periods.

4.3.2. Songpan-Ganze Terrane

[25] The Tibetan crustal conductor (TCC) is located in the crust with a resistivity of approximately 5 Ωm, and is underlain by a more resistive region. The TCC is required by the high values of φ_{TM} and φ_{TE} at periods of 100–10,000 s from distances of 100–500 km (Figure 4). Figure 5 shows the phase responses at TBT640 and the fit of the model in Figure 7. To demonstrate that the data are sensitive to geoelectric structure beneath the conductive layer, the resistivity of the underlying layer was perturbed from the 10 Ωm contour to a depth of 200 km. Figure 5 shows that when the lower-crust and upper mantle resistivity is raised to 100 Ωm, both φ_{TM} and φ_{TE} decrease significantly (Model E) at periods longer than 300 seconds. Similarly when the lower-crust and upper mantle resistivity is reduced to 3 Ωm, a significant increase in phase is observed (Model H) and the fit to both φ_{TM} and φ_{TE} becomes unacceptable beyond 300 seconds. The same behavior was also observed in the phase data at other stations in the Songpan-Ganze terrane, most clearly at TBT637 and TBT643. While perturbing the model can illustrate the sensitivity of the MT data to a feature in the model, it is important to evaluate other models through the use of constrained inversions. To do this, the inversion was restarted from the perturbed model, with the resistivity fixed in the perturbed region. With the low resistivity model (H), the inversion was unable to find a model that could fit the data (Figure 5). Thus models with low resistivity upper mantle are inconsistent with the data. This arises because the TE mode data require an increase in resistivity below the TCC. In contrast, when the resistive zone was fixed, the inversion was successful at fitting to the data through making the resistivity of the TCC lower than in Figure 7. This exercise was repeated for resistivity values of 300 and 1000 ohm-m and each case, attempting to fit the data forced

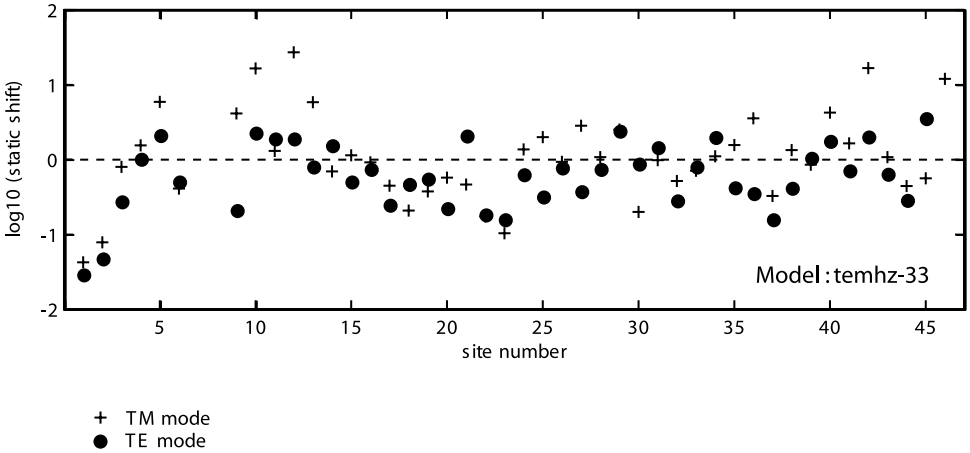

Figure 9. Static shift coefficients for the TE and TM mode data for the inversion shown in Figure 7.

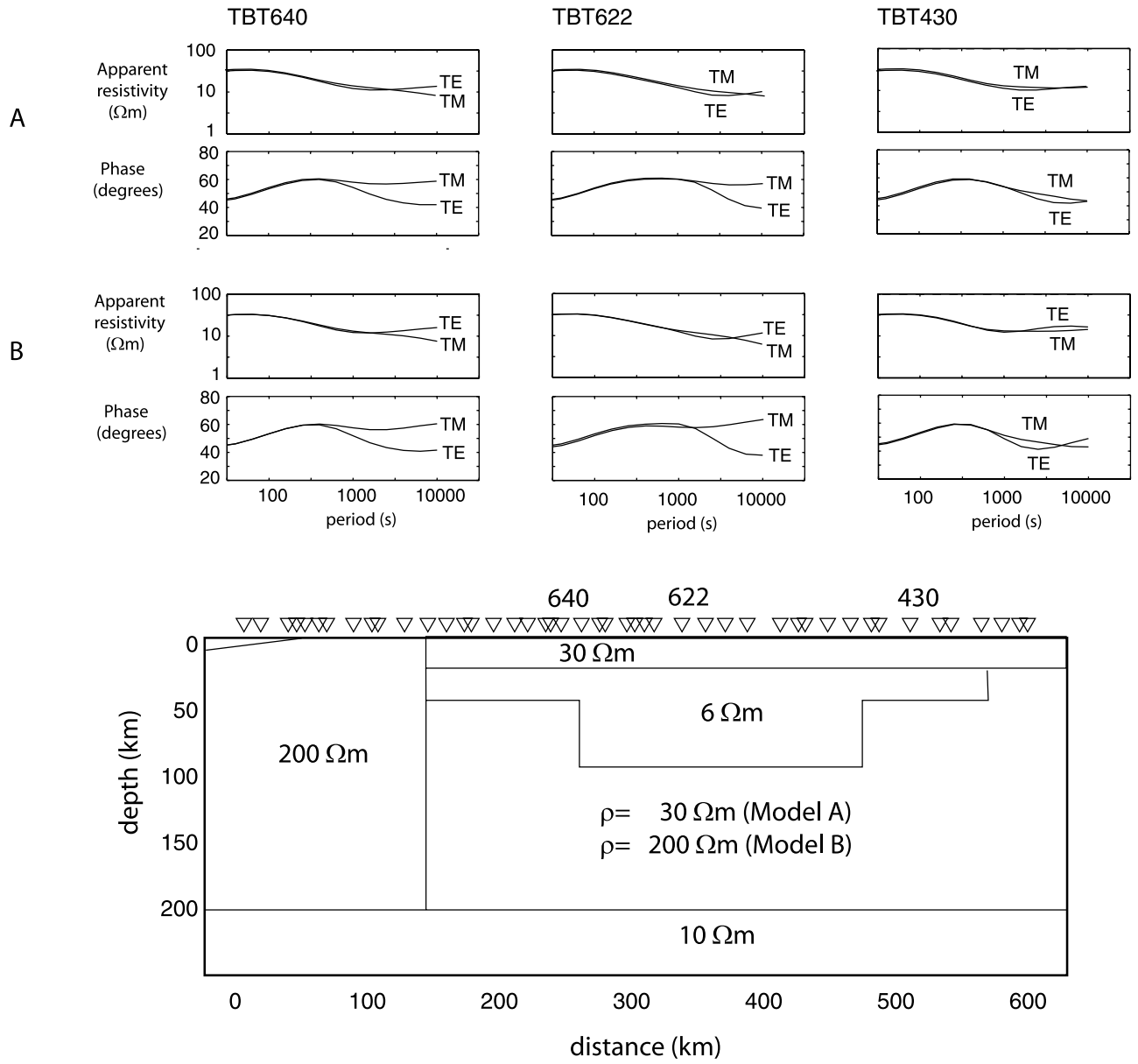

Figure 10. Synthetic MT responses of 2-D resistivity models at sites TBT640, TBT622 and TBT430.

the inversion to make the TCC even lower in resistivity. Thus while a high resistivity upper mantle cannot be excluded, it requires a very low resistivity within the TCC. These values are unphysical, suggesting that the MT data favor upper mantle resistivities below 300 ohm-m.

4.3.3. Northern Qiantang Terrane

[26] The TCC is also present in the Songpan-Ganze terrane, with the top shallowing to 20 km at 34°N (stations TBT622 and TBT619). The conductance of the TCC is greater than in the Songpan-Ganze terrane and it appears to extend to the base of the crust. The location of the lowest resistivity in the Tibetan crust at 34°N is required by the reversal in T_{zy} data and the high values of φ_{TM} at this location. Figure 5 shows the effect on response at TBT622 due to a change in resistivity from the base of the conductor to a depth of 200 km. Since the conductance is higher than in the Songpan-Ganze terrane, the responses begin to diverge at a longer period (1000 s) than at TBT640. The three model responses suggest that the MT data at TBT622 are sensitive to upper mantle resistivity. At this station, the results of the constrained inversion also show that the crustal conductor must be underlain by a more resistive upper mantle. The resistive upper mantle (100–300 ohm) is again somewhat consistent with the data, if the TCC is made lower in resistivity.

4.3.4. Southern Qiangtang Terrane

[27] The TCC begins at a depth of 20–30 km, as in the northern Qiangtang terrane. This zone extends to upper mantle depths, but the conductivity in this zone is lower than the northern Qiangtang terrane, typically around 10 Ωm. Data coverage in this region is not ideal, since long-period and broadband MT data were not collected at coincident sites. However, the ridge of high φ_{TM} has lower peak values in this area (<60° from 100 to 1000 s), indicating higher crustal resistivities than to the north. The reversal in the vertical magnetic field also requires an

increase in crustal resistivity compared to the northern Qiangtang terrane. Figure 5 show the phase data at TBT430, a typical long period site and indicate that the MT phase data are sensitive to the resistivity of the lower crust and upper mantle. The constrained inversions reveal again that a low resistivity upper mantle (3 ohm-m) is incompatible with the data. However, a resistive upper mantle gives an improved fit to the data.

[28] A range of additional constrained inversions were also undertaken, and gave results that were broadly similar to those described above. Resistivities below 3 Ωm for sub-TCC structure are inconsistent with the data, especially the φ_{TE} data. Resistivities in this zone above 300 ohm-m are a little more compatible, but result in unphysically low crustal resistivities. In summary, the sensitivity analysis shows that the data require that the TCC is underlain by a more resistive upper mantle, with a resistivity in the range 10–300 ohm-m. Higher resistivities can be permitted, but require a very low resistivity with the TCC. The TCC is thickest beneath the northern Qiangtang terrane. Models that attempt to fit the data through variable resistivity of a layer with fixed thickness produced unreasonably low resistivities.

4.4. Two-Dimensional Synthetic Inversions

[29] As an additional test of resolution beneath the TCC, synthetic data were generated for the models in Figure 10 and contaminated with both Gaussian noise and static shifts. Using the same inversion parameters as for the real data, the models in Figure 11 were obtained by inverting the synthetic data. The spatial extent, depth and resistivity of the TCC is well recovered, and there is clearly sensitivity to the resistivity below the TCC. The static shift coefficients estimated by the inversions are shown in Figure 11 for one model. The values are close to the true coefficients, and values obtained by down-weighting apparent resistivity, and using direct estimation in the inversion, are very similar.

4.5. Three-Dimensional Forward Modeling

[30] As described above, TE data must be included with care as they can be more sensitive to 3-D effects than the equivalent TM mode data. The fact that the TE and TM data can be fit with a 2-D model is one indication that 3-D effects are not serious. However, the PASSCAL data have indicated that the anomalous seismic properties are confined to a body of finite east-west extent [*McNamara et al.*, 1997]. To determine how 3-D effects could influence the 600-line MT data, a 3-D geoelectric model was generated using the 2-D model in Figure 10 as a basis. The TCC in the model was terminated at a range of east-west distance from the profile. The forward response of the model was computed using the 3-D modeling algorithm of *Mackie et al.* [1994]. The phase response at station TBT622 are shown in Figure 12 for a range of models. When the conductive features extend to 500 km east and west, a departure from the 2-D response is only observed at periods beyond 5000 s. The zone of *S* wave attenuation described by *McNamara et al.* [1997] extended at least 300 km east and 500 km west of the Lhasa-Golmud highway. When these dimensions are applied to the Tibetan Crustal conductor, a departure from the 2-D response is observed at 3000 s. Note that the change in response is greatest in the TE mode, and the 3-D effect is to make ρ_{TE} decrease at the longest periods. The physical origin of this effect is the presence of electric charges on the east and west ends of the conductors, and is very similar to that previously discussed for ρ_{TM} in the context of 2-D forward modeling. The 3-D model, with finite strike length, thus produces higher values of φ_{TE} at long periods, compared to the true 2-D model. This behavior implies that if 3-D effects are present in the field data, then a 2-D interpretation will give a model that is less resistive (more conductive) than the true model. However, given the along strike dimensions inferred from seismic data, this effect is restricted to the longest periods, and is likely small in magnitude.

4.6. Summary of Modeling and Inversion

[31] The modeling and inversion presented in this section have shown that the Tibetan crustal conductor (TCC) is present in the mid and lower crust from the Kunlun Shan to the southern end of the profile, with the highest conductance in the northern Qiangtang terrane. In addition, the upper mantle more resistive than TCC. The resistivity is greater than 10 ohm-m, with the preferred resistivity less than 100 ohm-m.

5. Interpretation of Resistivity Models

5.1. Active Tectonics and Shallow Structure of the Kunlun Shan and Qaidam Basin

[32] The TCC underlies the entire north-south extent of the Tibetan Plateau and terminates at the Kunlun fault. If this represents a rheologically weak layer, then its termination at the Kunlun fault is highly significant. Both geodetic data and recent earthquakes show that the Kunlun fault accommodates the eastward extrusion of the upper Tibetan crust as north-south convergence between India and Asia continues at depth [*Wang et al.*, 2001; *Lin et al.*, 2002]. The weak midcrustal layer effectively decouples the upper and lower portions of the lithosphere, with this decoupling extending northward as far as the Kunlun fault. Figure 13 shows the upper 20 km of the model in Figure 7. The sedimentary units of the Qaidam Basin are imaged as a low resistivity section 3–4 km thick, in agreement with well log information [*Metevier et al.*, 1998]. The resistivity is lowest in the bottom section of the basin, which might reflect saline aquifers confined to the base of the sedimentary basin. The low resistivity basin sediments pinch out at location of +50 km, coincident with the northernmost range of the Kunlun Shan. Within the Kunlun Shan the upper crustal units have generally high resistivities (>1000 Ωm), and regrettably the 600-line MT stations are not ideally spaced to trace shallow structures with confidence. This is compounded by the fact that a number of these MT stations have highly distorted electric fields, and were also contaminated by noise from the Golmud hydroelectric plant. Despite these drawbacks, a series of interfaces dipping to the south are imaged. In magnetotelluric studies of similar tectonic settings elsewhere, low resistivity units in the footwall of the thrust fault have been imaged [*Bedrosian et al.*, 2001; *Park et al.*, 2003]. On the 600-line a south dipping low resistivity zone is imaged, (distances 50–80 km and depths 5–10 km). This might represent underthrust sedimentary units but the geometry cannot be adequately resolved, owing to the data problems outlined above.

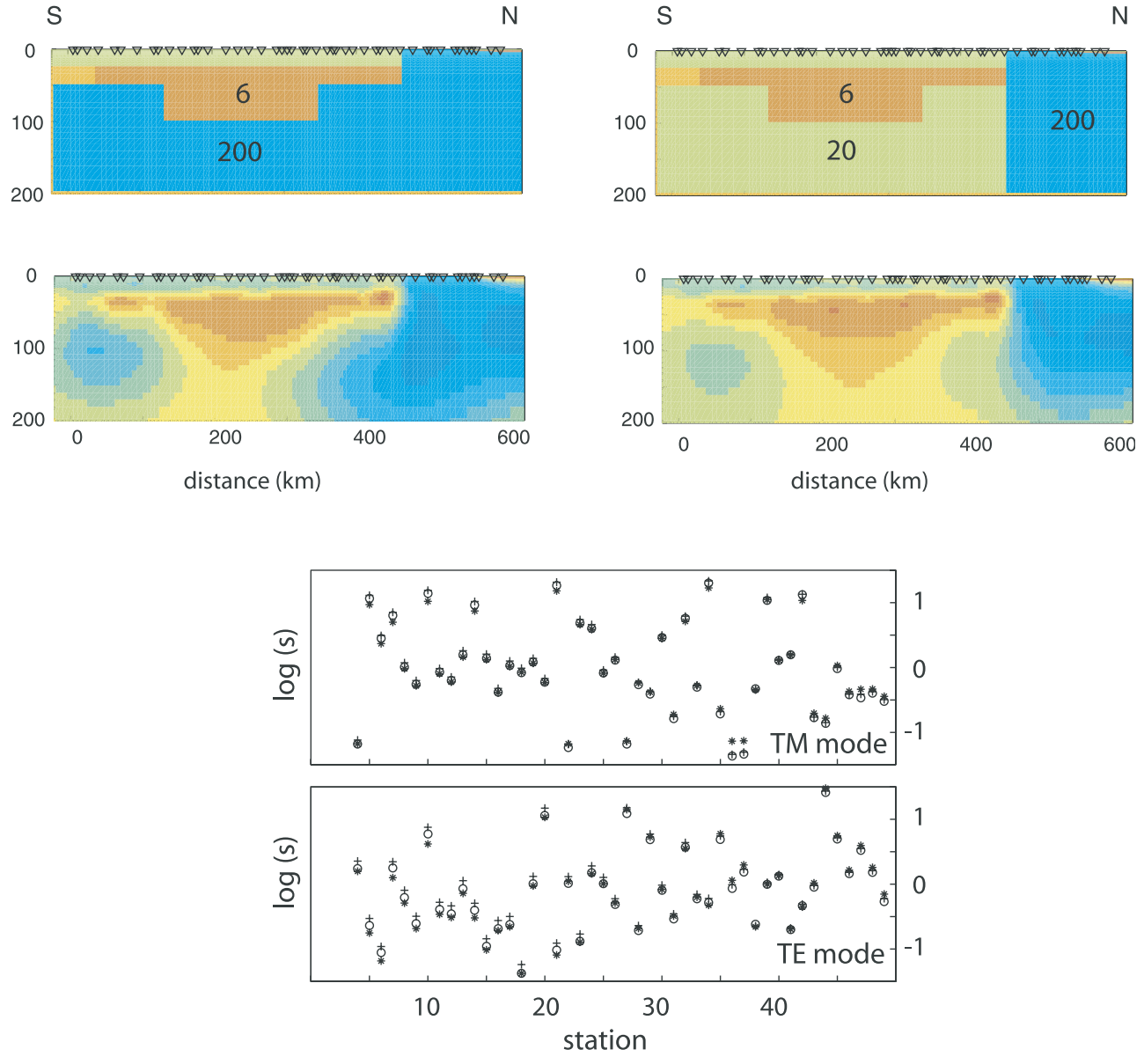

Figure 11. Inversion of synthetic MT data generated for the models in Figure 10. Data were contaminated with 10% noise in apparent resistivity and an equivalent amount in phase. Static shifts coefficients were applied to apparent resistivity with a Gaussian distribution having a width of $\log_{10}$ (static) = 0.7. The original static shifts coefficients (open circle) are plotted along with the values recovered using down weighted resistivity (asterisk) and direct estimation in the inversion (plus symbol) for the model with a 200 Ωm upper mantle. The TM mode static shift coefficients for both estimation methods have been multiplied by a factor of 2 in this figure.

[33] At the longitude of the 600-line location, the Kunlun fault comprises two major branches and south dipping resistivity contrasts are coincident with both. *Mock et al.* [1999] suggested that unroofing has occurred in the Kunlun Shan with a wedge of midcrustal rocks being exhumed between the two strands of the Kunlun fault. The MT model is certainly consistent with this mechanism, but station spacing does not permit details to be resolved as in other more detailed fault zone studies [*Unsworth et al.*, 2000]. To the south of the Kunlun Shan, a thin cover of low resistivity sediments commences at 150 km and thickens to the south across the Songpan Ganze terrane, reaching a maximum thickness of 5–6 km at a distance of 250 km. The major contrast in resistivity between the resistive Kunlun Shan and the conductive basin in the Songpan-Ganze terrane gives rise to the pronounced reversal in the real component of T_{zy} in the period band 1–10 s at a distance of 150 km.

5.2. Tibetan Crustal Conductor and Comparison With Seismic Results

[34] The Tibetan Crustal Conductor (TCC) imaged with these data is at a similar depth to other locations on the Tibetan Plateau [*Wei et al.*, 2001]. However, the maximum conductance is significantly higher than to the west (500-

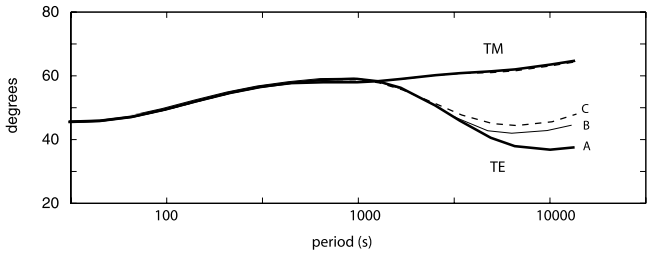

Figure 12. Synthetic MT responses of 3-D geoelectric models for northern Tibet at site TBT622. Model "A" is a 2-D model based on model "B" in Figure 10. The Tibetan crustal conductor is terminated at ±300 km in model "B." In "C" the conductor extends 300 km east and 500 km west of the profile. Note that the TE mode is most strongly influenced by the 3-D structure.

line [*Wei et al.*, 2001]) and is comparable to southern Tibet [*Chen et al.*, 1996]. In northern Tibet, the crust is 60–70 km thick [*Owens and Zandt*, 1997; *Vergne et al.*, 2002] and the TCC appears to be located within the lower crust. Interconnected fluids, probably cause the high conductivity (either partial melt or aqueous fluids), although other explanations are possible [*Li et al.*, 2003]. A bulk resistivity of 6 Ω-m requires a melt fraction in the range 2–6% depending on the resistivity of the melt [*Li et al.*, 2003]. In some of the constrained inversions previously described, the MT data were shown to be consistent with a resistive upper mantle if the crustal resistivity was below 1 Ωm. If due to the presence of interconnected partial melt, this would likely require a melt fraction in excess of 20%, which is likely physically unstable [*Li et al.*, 2003].

[35] How does the MT model compare with crustal models derived from seismic data? The analysis of the PASSCAL data by *Owens and Zandt* [1997] showed that the Qiangtang and Songpan-Ganze terranes were characterized by low seismic velocity in the lower crust and a zone of inefficient S-wave propagation in the upper mantle. These properties imply the presence of high temperatures and partial melting in the lower crust and upper mantle. While these seismic anomalies are centered to the west of the Lhasa-Golmud highway, they are well defined at the longitude of the 600-line. *Owens and Zandt* [1997] also suggested that the crust was thinnest, and the velocities lowest, beneath the Songpan-Ganze terrane. However, other analyses of the PASSCAL data set, combined with additional Sino-French seismic data showed that quite different velocity models can be derived for northern Tibet. *Vergne et al.* [2002] demonstrated that depending on the choice of converted phases used, (1) the model of *Owens and Zandt* [1997], (2) a model with a thicker crust but high Poisson's ratio in the lowest 20 km, or (3) a thicker crust with normal Poisson's ratio could be required. In interpreting the MT data from the Qiangtang and Songpan Ganze terranes, this range of seismic interpretations must be considered. The MT results in this paper are consistent with the model of *Owens and Zandt* [1997] in that both require a lower crust that has a high fluid content (presumably because it is hot) and which extends north to the Kunlun fault. Regrettably, the 600-line terminates at the Bangong-Nuijiang suture and the continuation of the INDEPTH magnetotelluric data is offset west at this point to the 500-line [*Wei et al.*, 2001]. However, the MT data are not entirely in agreement with the model of *Owens and Zandt* [1997]. The magnetotelluric data detect the lowest resistivities (and by inference highest melt fractions) in the middle crust beneath the northern Qiangtang terrane (and not the Songpan-Ganze terrane).

[36] The MT results are broadly consistent with *Owens and Zandt* [1997]. However, *Vergne et al.* [2002] favor a model with very limited partial melting in the crust. One possible way to reconcile these data is to recognize the relatively low melt fractions (2–6%) are required to explain the MT data in northern Tibet [*Li et al.*, 2003]. Laboratory analyses have shown that at this melt fraction, both seismic velocities and Poisson's ratio will be close to the value a dry rock [*Schmelling*, 1985]. In the context of the study area, *Rogers and Schwartz* [1998] showed that 2% partial melt in the upper mantle beneath northern Tibet might only raise Poisson's ration from 0.27 to a value in the range 0.28–0.29. Xenolith studies have shown that the lower Qiangtang crust is both hot and dry [*Hacker et al.*, 2000]. Thus the MT model could be reconciled with the seismic model of *Vergne et al.* [2002] if the lower crust is essentially at melting point with enough melt to lower electrical resistivity but not significantly raise Poisson's ratio. Another factor to be

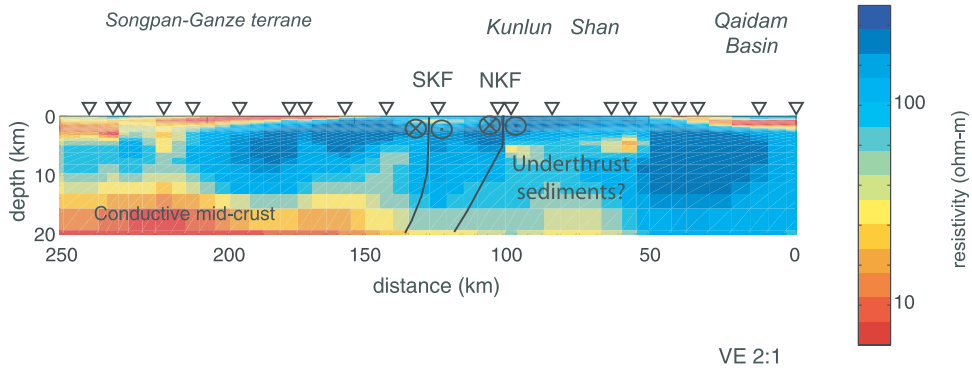

Figure 13. Detailed geoelectric model of northern part of 600-line MT profile with vertical exaggeration of 2:1. Note that the color scale is different to that used in Figure 7. NKF and SKF denote the northern and southern branches of the Kunlun fault. Fault locations at depth are based on *Tapponnier et al.* [2001] and *Mock et al.* [1999].

considered in reconciling the MT and seismic models for the Qiangtang and Songpan-Ganze crust is that the amount of melting is decreasing rapidly across the Songpan-Ganze terrane and was only sampled at the southern of the seismic profiles of *Vergne et al.* [2002]. In addition the study of *Galve et al.* [2002] was located around 500 km to the east of the 600-line.

[37] Is the distribution of low resistivity in the crust of the northern Tibetan Plateau due to factors other than partial melt? *Kapp et al.* [2000] suggest that the Songpan-Ganze terrane was underthrust a significant distance southward beneath the Qiangtang terrane when the Jinsha River formed. To the west of the Lhasa-Golmud highway, these rocks are now exposed at the surface in the Qiangtang anticlinorium west of Shuang He. Since this emplacement would have introduced significant water into the crust, this could have initiated crustal melting in the northern Qiangtang terrane. In Figure 14a, the inferred geometry of the Songpan-Ganze terrane at depth from *Yin and Harrison* [2000] can be seen to be coincident with the lowest crustal resistivities below 20 km depth. The Tibetan Crustal Conductor might have developed as melting propagated throughout the mid and lower crustal portion of the Songpan Ganze terrane owing to lower melting point that resulted from the enhanced fluid content [*Beaumont et al.*, 2001]. It is also possible that the fluid content of the Songpan-Ganze Terrane contributes to the lower resistivity of this feature. One factor that is not explained by this hypothesis, is the fact that such low resistivities are not observed to the west on the 500-line [*Wei et al.*, 2001] where the underthrust Songpan-Ganze Terrane is also present. In addition, the absence of a geoelectric expression at the Jinsha River suture is enigmatic.

[38] A range of geodynamic models for the Tibetan Plateau suggest that lower crustal flow could be a significant mechanism for achieving mass balance [*Clark and Royden*, 2000]. Crustal flow can occur by high temperature creep and does not require a fluid phase, although a fluid phase will significantly enhance the rate of creep by reducing the viscosity. The Tibetan Crustal Conductor imaged on this profile may well represent a channel of lower crustal flow that is transporting crustal material to the east. The absence of a pronounced low resistivity feature to the west suggests that this process may become more active on the 600-line compared to the upstream location of the 500-line to the west [*Wei et al.*, 2001].

5.3. Upper Mantle Structure

[39] Owing to the presence of the Tibetan Crustal Conductor, the MT data provide less rigorous constraints on upper mantle structure beneath northern Tibet. However, the data analysis presented in this paper suggests that the upper mantle beneath northern Tibet is in the range 10–100 Ωm. North-south variations in upper mantle resistivity cannot be resolved by the data. The resistivity of the continental uppermost mantle is difficult to determine, due to the presence of the almost ubiquitous lower crustal conducting layer. Estimates by many researchers suggest 100 Ωm as a minimum value with typical values 1–2 orders of magnitude higher [*Jones*, 1999]. Thus the 600-line MT data appear to image a low resistivity upper mantle beneath northern Tibet. These values strongly suggest elevated temperatures and perhaps partial melting, although other mechanisms for lowering the resistivity of the upper mantle have been suggested [*Leibecker et al.*, 2002]. Underthrusting of cold Asian lithosphere would result in resistivities of 100 Ωm or greater. The apparent absence of high resistivities in the upper mantle south vicinity of the Jinsha River suture and to the south suggests that Asian lithosphere does not extend this far (or if it has then the resistivity of the lithosphere has been dramatically reduced by an undetermined mechanism).

[40] Upper mantle structure is reasonably consistent between the seismic and MT data sets on the Lhasa-Golmud highway. *Wittlinger et al.* [1996] reported a low-velocity zone in the upper mantle at depths of 200–300 km around 34°N. This is deeper than the mantle low-resistivity zone detected with the magnetotelluric data. However, both data sets could be imaging different portions of the same upper mantle feature. Alternatively, it might reflect the limited vertical resolution of the analysis technique used by *Wittlinger et al.* [1996], and it is possible that the low velocity zone is shallower than previously thought [*Tapponnier et al.*, 2001]. *Kind et al.* [2002] derived receiver functions of the combined INDEPTH, Sino-French and PASSCAL data set and showed that south dipping events could be identified in the upper mantle beneath northern Tibet. This structure is in the location anticipated for the top of Asian lithosphere being subducted southward beneath northern Tibet.

5.4. Delamination and Upwelling Asthenosphere?

[41] Can the geoelectric structure derived from the INDEPTH MT data discriminate between the competing geodynamic models proposed for northern Tibet? In the following sections, the two main classes of models will be evaluated in regard to the geoelectric model derived from the MT data (Figure 14).

[42] Many geodynamic models of the Tibetan Plateau invoke continuum deformation of the lithosphere and assume an inherently weak rheology for the Tibetan lithosphere [*England and Houseman*, 1989; *Zhao and Morgan*, 1987]. Some models in this class suggest that a thickened Tibetan lithosphere become unstable and delaminated, producing a localized upwelling of the asthenosphere [*Molnar*, 1988]. Elevated temperatures and perhaps partial melting in the upper mantle would be a natural consequence of this process, and would produce low electrical resistivities [*Partzsch et al.*, 2000]. As mantle-derived melts migrate upward through the crust, they initiate crustal melting and pervasive low resistivity results in the lower crust. The model in Figure 14a is broadly consistent with this class of models, since it implies the upper mantle has a relatively low resistivity (10–30 Ωm). This resistivity value is more consistent with a hot upper mantle containing a few percent partial melt than with underthrust Asian lithosphere beneath northern Tibet.

5.5. Subduction of Asian lithosphere

[43] The other main class of geodynamic models for the Tibetan Plateau propose a rigid, cold lithosphere. In this class of models, the crust and lithosphere was thickened by under thrusting and stacking [*Tapponnier et al.*, 2001]. This class of model is shown schematically in Figures 14b and 14c, with the depth of subducting Asian lithospheric mantle

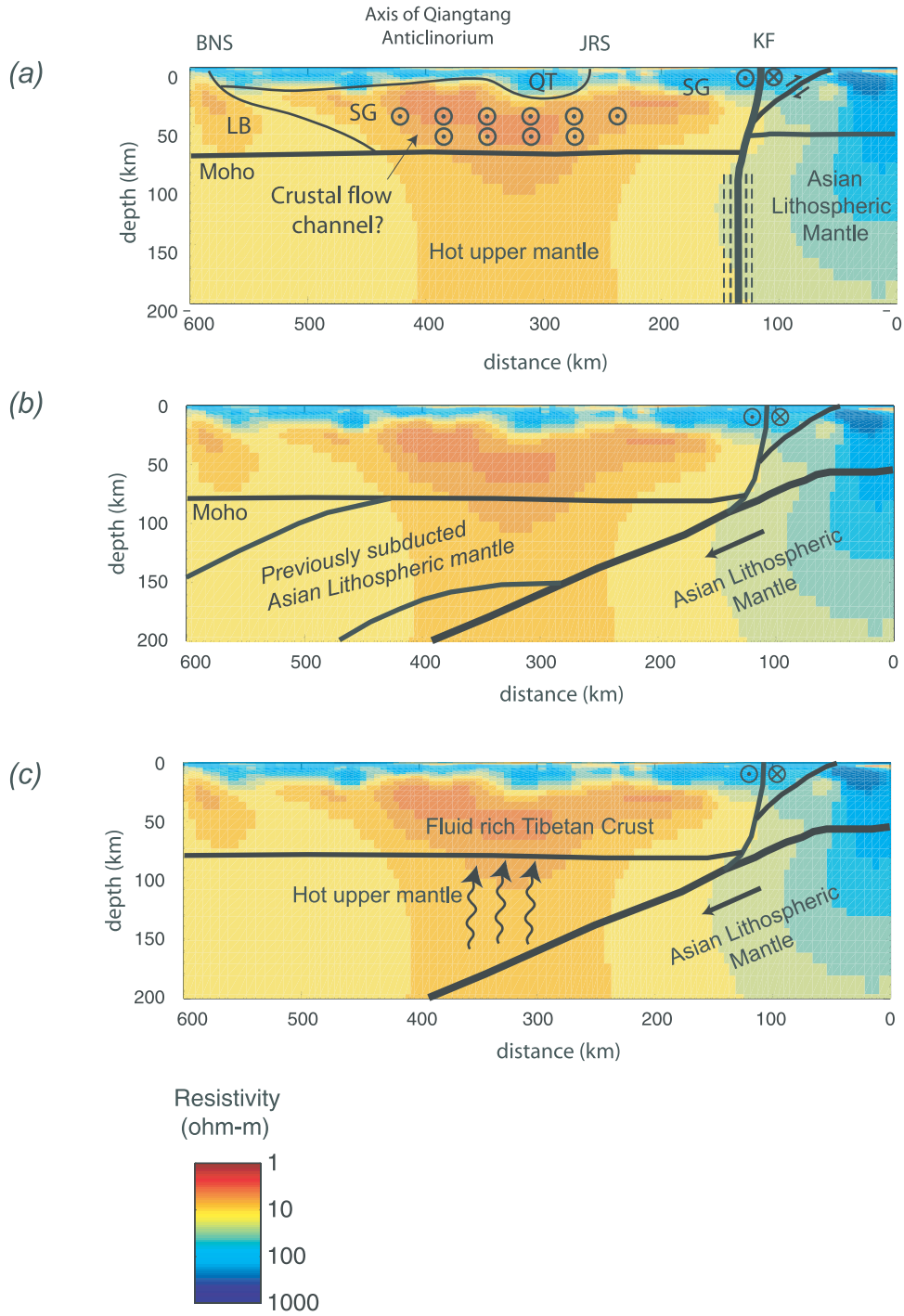

Figure 14. Cartoon showing possible crustal and upper mantle structures for northern Tibet. (a) The northern margin of Tibet is a major shear zone with minimal subduction. Model is based on that of *Owens and Zandt* [1997] with crustal structure adapted from *Yin and Harrison* [2000]. (b) Asian lithospheric mantle is subducted beneath northern Tibet as proposed by *Tapponnier et al.* [2001]. Previous subduction events have imbricated slices of Asian lithosphere beneath the entire northern Tibetan Plateau. (c) Alternative geometry for subduction of Asian lithosphere with a wedge of hot upper mantle overlying the subducting Asian lithosphere. In both Figures 14b and 14c the location of the Asian lithospheric mantle is taken from *Kind et al.* [2002]. Abbreviations are as follows: BNS, Bangong-Nuijiang suture; JS, Jinsha River Suture; KF, Kunlun fault; LB, Lhasa Block; QT, Qiangtang terrane; SG, Songpan Ganze terrane.

taken from *Kind et al.* [2002]. This model predicts generally high resistivities in the upper mantle beneath northern Tibet that are not observed. Underthrusting of Asian lithosphere could initiate melting as subducted fluids lowered the melting point and melt would rise into the upper plate and initiate limited crustal melting. The axis of highest conductivity at 34°N is in the location that might be expected for such a scenario [*Yin and Harrison*, 2000; *Tapponnier et al.*, 2001]. While few Plio-Pleistocene volcanic rocks are found close to the Lhasa-Golmud highway, a series of volcanic centers have been mapped to the west, along strike from the high conductivity feature at 34°N [*Turner et al.*, 1993; *Hacker et al.*, 2000]. This model requires that the Songpan-Ganze terrane be underlain by Asian lithosphere, which would be expected to be relatively cold and electrically resistive. However, the MT data analysis described above showed that electrical resistivities in the lower crust/upper mantle of the Songpan-Ganze terrane are in the range 10–30 Ωm. This value is far lower than would be expected for relatively cold Asian lithosphere being underthrust beneath northern Tibet and appears to be inconsistent with the continental subduction as proposed by *Tapponnier et al.* [2001]. The only way to reconcile these observations would be if the underthrusting of Asian lithosphere has produced a network of conductive zones which would lower the resistivity of these rocks from their values beneath the Qaidam Basin to the observed value. It should also be noted that the upper mantle resistivity beneath northern Tibet (10–30 Ωm) is too high to be consistent with pervasive partial melting, but could be explained by interconnected melt fractions of the order of a few percent [*Partzsch et al.*, 2000]. Figure 14c shows an alternative scenario for subduction of Asian lithosphere beneath northern Tibet. In this model, a wedge of relatively hot upper mantle overlies the subducting lithosphere with the depth defined by the receiver function analysis of *Kind et al.* [2002]. Melts derived from the descending lithosphere rise and cause limited additional melting in the Tibetan crust, centered at 34°N. In this geometry, the resistive lithosphere would be masked by the conductive upper mantle and thus it could not be readily detected by the existing MT data.

6. Conclusions

[44] The magnetotelluric data described in this paper have constrained the geoelectric structure of the lithosphere beneath the northern Tibetan Plateau. The middle and lower crust of the Songpan-Ganze and Qiangtang terranes is conductive, with the most conductive zone centered in the northern Qiangtang terrane at 34°N. This conductive zone is probably due to high temperatures with small amounts of partial melting. This is consistent with seismic observations of only slightly elevated Poisson's ratio and a hot, dry lower crust inferred from geochemical analysis of xenoliths. This Tibetan crustal conductor could represent a channel of lower crustal flow. The upper mantle has a relatively uniform electrical resistivity (10–30 Ωm) from the Kunlun Shan to the Bangong-Nuijiang suture. North of the Kunlun Shan, the upper mantle is more resistive with values typical of stable continental lithosphere.

[45] Can this geoelectric model require or exclude any of the geodynamic models that have been proposed for Tibet? The conductive upper mantle south of the Kunlun Shan is clearly inconsistent with models of whole-scale underthrusting of Asian lithosphere since this would predict uniform, high resistivity values at this location. If Asian lithosphere extends beyond this point then it must have been sufficiently altered to produce the observed low resistivity. Thus the resistivity of the lower crust and upper mantle in the Qiangtang and Songpan-Ganze terranes are more consistent with geodynamic models requiring continuum, viscous deformation in the lower crust and upper mantle. This would likely produce partial melting in the upper mantle (and to a degree the lower crust) and would account for the low resistivities observed. Thus the preferred model is that with Asian lithosphere underthrusting northern Tibet as far as the Kunlun fault, and a thin lithosphere with shallow asthenosphere to the south. It must be stressed that these models are derived from magnetotelluric measurements on a single north-south transect. Additional magnetotelluric profiles to the east and west are needed to validate these models. Another possible model could satisfy the MT data and seismic observations of southward dipping Asian lithosphere beneath the profile [*Kind et al.*, 2002]. The MT data exclude Asian lithosphere being present directly under the Moho. However, there might exist a mantle wedge that is hot and partially molten (the top of which is detected by the MT), and underlain by subducting Asian lithosphere at depth.

[46] **Acknowledgments.** Financial support was provided by the Continental Dynamics Program at the National Science Foundation (EAR-9614590), China University of Geoscience (Beijing), Chinese Ministry of Land and Resources and the National Science Foundation of China. This fieldwork was made possible through the help of many local people. The drivers of the Fifth Brigade are thanked for their safe driving and good sense of humor. We thank David Kay for his heroic efforts during the 1999 field campaign. Many scientific discussions with the INDEPTH group are acknowledged, especially the many insightful comments and ideas received from the late Doug Nelson. The paper benefited from reviews by Henri Brasse and Stephen Park and comments from Karsten Bahr.

References

Argand, E. (1924), La tectonique de l'Asie, *Int. Geol. Congr. Rep. Sess.*, *13*, 170–373.

Arnaud, N. O., P. Vidal, P. Tapponnier, P. Matte, and W. Deng (1992), The high K_2O volcanism of Northwestern Tibet: Geochemistry and tectonic implications, *Earth Planet. Sci. Lett.*, *111*, 351–367.

Beaumont, C., R. A. Jamieson, M. H. Nguyen, and B. Lee (2001), Himalayan tectonics explained by extrusion of a low-viscosity crustal channel coupled to focused surface denudation, *Nature*, *414*, 738–742.

Bedrosian, P. A., M. J. Unsworth, and F. Wang (2001), Structure of the Altyn Tagh Fault and Daxue Shan from magnetotelluric surveys: Implications for faulting associated with the rise of the Tibetan Plateau, *Tectonics*, *20*, 474–486.

Chen, L., J. R. Booker, A. G. Jones, N. Wu, M. J. Unsworth, W. Wenbo, and H. Tan (1996), Electrically conductive crust in southern Tibet from INDEPTH magnetotelluric surveying, *Science*, *274*, 1694–1696.

Chen, W. P., C. Y. Chen, and J. L. Nabelek (1999), Present day deformation of the Qaidam Basin with implications for intra-continental tectonics, *Tectonophysics*, *305*, 165–181.

Clark, M., and L. Royden (2000), Topographic ooze: Building the eastern margin of Tibet by lower crustal flow, *Geology*, *28*, 703–706.

Coward, M. P., W. S. F. Kidd, P. Yun, R. M. Shackelton, and Z. Hu (1988), The structure of the 1985 Tibet Geotraverse, Lhasa to Golmud, *Philos. Trans. R. Soc. London, Ser. A.*, *327*, 307–336.

Dewey, J., and K. Burke (1973), Tibetan, Variscan and Precambrian reactivation: Product of continental collision, *J. Geol.*, *81*, 683–692.

Dewey, J., R. M. Shackelton, C. Chang, and Y. Sun (1988), The tectonic evolution of the Tibetan Plateau, *Philos. Trans. R. Soc. London., Ser. A.*, *327*, 379–413.

Egbert, G. D. (1997), Robust multiple-station magnetotelluric data processing, *Geophys. J. Int.*, *130*, 475–496.

England, P. C., and G. A. Houseman (1989), Extension during continental convergence, with application to the Tibetan Plateau, *J. Geophys. Res*, *94*, 17,561–17,579.

Galve, A., A. Hirn, J. Mei, J. Gallart, B. de Voogd, J. C. Lepine, J. Diaz, W. Youxue, and Q. Hui (2002), Modes of raising northeastern Tibet probed by explosion seismology, *Earth Planet. Sci. Lett.*, *203*, 35–43.

Griot, D. A., J. P. Montagner, and P. Tapponnier (1998), Phase velocity structure from Rayleigh and Love waves in Tibet and its neighboring regions, *J. Geophys. Res.*, *103*, 21,215–21,232.

Groom, R. W., and R. C. Bailey (1989), Decomposition of magnetotelluric impedance tensors in the presence of local three-dimensional galvanic distortion, *J. Geophys. Res.*, *94*, 1913–1925.

Hacker, B. R., E. Gnos, L. Ratschbacher, M. Grove, M. McWilliams, S. Sobolev, J. Wan, and Z. Wu (2000), Hot and dry deep crustal xenoliths from Tibet, *Science*, *287*, 2463–2466.

Hirn, A., M. Sapin, J. C. Lepine, J. Diaz, and J. Mei (1997), Increase in melt fraction along a north south traverse below the Tibetan Plateau: Evidence from seismology, *Tectonophysics*, *273*, 17–30.

Jones, A. G. (1988), Static shift of magnetotelluric data and its removal in a sedimentary basin environment, *Geophysics*, *53*, 967–978.

Jones, A. G. (1999), Imaging the continental upper mantle using electromagnetic methods, *Lithos*, *48*, 57–80.

Jones, A. G., A. D. Chave, G. D. Egbert, D. Auld, and K. Bahr (1989), A comparison of techniques for magnetotelluric response function estimates, *J. Geophys. Res.*, *94*, 14,201–14,213.

Kapp, P., A. Yin, C. E. Manning, M. Murphy, T. M. Harrison, M. Spurlin, D. Lin, X. Deng, and C. Wu (2000), Blueschist-bearing metamorphic core complexes in the Qiangtang block reveal deep crustal structure of northern Tibet, *Geology*, *28*, 19–22.

Kidd, W. S. F., and P. Molnar (1988), Quaternary and Active faulting observed on the 1985 Academica Sinica-Royal Society Geotraverse of Tibet, *Philos. Trans. R. Soc. London, Ser. A*, *327*, 337–363.

Kind, R., et al. (2002), Seismic images of crust and upper mantle beneath Tibet: Evidence for Eurasian plate subduction, *Science*, *298*, 1219–1221.

Kosarev, G., R. Kind, S. V. Sobolev, X. Yuan, W. Hanka, and O. Oreshin (1999), Seismic evidence for a detached Indian lithospheric mantle beneath Tibet, *Science*, *283*, 1306–1309.

Ledo, J., P. Queralt, A. Martí, and A. G. Jones (2002), Two-dimensional interpretation of three-dimensional magnetotelluric data: An example of limitations and resolution, *Geophys. J. Int.*, *150*, doi:10.1046/j.1365-246X.2002.01705.x, 127–139.

Leibecker, J., A. Gatzemeier, M. Honig, O. Kuras, and W. Soyer (2002), Evidence of electrical anisotropic structures in the lower crust and the upper mantle beneath the Rhenish Shield, *Earth Planet. Sci. Lett.*, *202*, 289–302.

Li, S., M. J. Unsworth, J. R. Booker, W. Wei, H. Tan, and A. G. Jones (2003), Partial melt or aqueous fluids in the Tibetan crust: Constraints from INDEPTH magnetotelluric data, *Geophys. J. Int.*, *153*, doi:10.1046/j.1365-246X.2003.01850.x, 289–304.

Lin, A., B. Fu, J. Guo, Q. Zeng, G. Dang, W. He, and Y. Zhao (2002), Coseismic strike-slip rupture length produced by the 2001 M_S = 8.1 central Kunlun earthquake, *Science*, *296*, 2015–2017.

Mackie, R. L., T. R. Madden, and J. T. Smith (1994), Three-dimensional electromagnetic modeling using finite difference equations: The magnetotelluric example, *Radio Sci.*, *29*, 923–935.

Matte, P., P. Tapponnier, N. Arnaud, L. Bourjot, J.-P. Avouac, P. Vidal, Q. Liu, Y. Pan, and Y. Wang (1996), Tectonics of western Tibet, between the Tarim and the Indus, *Earth Planet. Sci. Lett.*, *142*, 311–330.

McNamara, D. E., W. R. Walter, T. J. Owens, and C. J. Ammon (1997), Upper mantle velocity structure beneath the Tibetan Plateau from Pn travel time tomography, *J. Geophys. Res.*, *102*, 493–505.

McNeice, G. W., and A. J. Jones (2001), Multisite, multifrequency tensor decomposition of magnetotelluric data, *Geophysics*, *66*, 158.

Metevier, F., Y. Gaudemer, P. Tapponnier, and B. Meyer (1998), Northeastward growth of the Tibet Plateau deduced from balanced reconstruction of two depositional areas: The Qaidam and Hexi Corridor basins, China, *Tectonics*, *17*, 823–842.

Mock, C., N. O. Arnaud, and J. M. Cantagrel (1999), An early unroofing in northeastern Tibet?: Constraints from $^{40}Ar/^{39}Ar$ thermochronology on granitoids from the eastern Kunlun range (Qinghai, NW China), *Earth Planet. Sci. Lett.*, *171*, 107–122.

Molnar, P. (1988), A review of geophysical constraints on the deep structure of the Tibetan Plateau, the Himalayas and the Karakorum and their tectonic implications, *Philos. Trans. R. Soc. London, Ser. A*, *326*, 33–88.

Narod, B. B., and J. R. Bennest (1990), Ring-core fluxgate magnetometers for use as observatory variometers, *Phys. Earth Planet. Inter.*, *59*, 23–28.

Nelson, K. D., et al. (1996), Partially molten middle crust beneath southern Tibet: Synthesis of Project INDEPTH results, *Science*, *274*, 1684–1686.

Ni, J., and M. Barazangi (1983), High frequency seismic wave propagation beneath the Indian Shield, Himalayan Arc, Tibetan Plateau and surrounding regions: High uppermost mantle velocities and efficient S_n propagation beneath Tibet, *Geophys. J. R. Astron. Soc.*, *72*, 665–689.

Owens, T. J., and G. Zandt (1997), Implications of crustal property variations for models of Tibetan Plateau evolution, *Nature*, *387*, 37–43.

Park, S. K., S. Thompson, A. Rybin, V. Batalev, and R. Bielinski (2003), Structural constraints in neotectonic studies of thrust faults from the magnetotelluric method, Kochkor Basin, Kyrgyz Republic, *Tectonics*, *22*(2), 1013, doi:10.1029/2001TC001318.

Parkinson, W. D. (1962), The influence of continents and oceans on geomagnetic variations, *Geophys. J. R. Astron. Soc.*, *6*, 441–449.

Partzsch, G. M., F. R. Schilling, and J. Arndt (2000), The influence of partial melting on the electrical behavior of crustal rocks: Laboratory examinations, model calculations and geological interpretations, *Tectonophysics*, *317*, 189–203.

Rapine, R., F. Tilmann, M. West, J. Ni, and A. Rodgers (2003), Crustal structure of northern and southern Tibet from surface wave dispersion analysis, *J. Geophys. Res.*, *108*(B2), 2120, doi:10.1029/2001JB000445.

Rodi, W., and R. L. Mackie (2001), Nonlinear conjugate gradients algorithm for 2-D magnetotelluric inversion, *Geophysics*, *66*, 174–187.

Rogers, A. J., and S. Y. Schwartz (1998), Lithospheric structure of the Qingtang terrane, northern Tibetan Plateau, from complete regional waveform modeling: Evidence for partial melt, *J. Geophys. Res.*, *103*, 7137–7152.

Schmelling, H. (1985), Numerical models on the influence of partial melt on elastic and electric properties of rocks, 1. Elasticity and anelasticity, *Phys. Earth Planet. Inter.*, *41*, 34–57.

Shengye, Z., W. Sheng, and W. Jiaying (1996), Magnetotelluric sounding in the Qiangtang basin of Xizang (Tibet), *J. China Univ. Geosci.*, *21*, 198–202.

Tapponnier, P., Z. Xu, F. Roger, B. Meyer, N. Arnaud, G. Wittlinger, and Y. Jingsui (2001), Oblique stepwide rise and growth of the Tibetan Plateau, *Science*, *294*, 1671–1677.

Turner, S., C. Hawkesworth, J. Liu, N. Rogers, S. Kelly, and P. van Calsteren (1993), Timing of Tibetan Plateau uplift constrained by analysis of volcanic rocks, *Nature*, *364*, 50–54.

Unsworth, M. J., M. Eisel, G. D. Egbert, W. Siripunarvaporn, and P. A. Bedrosian (2000), Along-strike variations in the structure of the San Andreas Fault at Parkfield, California, *Geophys. Res. Lett.*, *27*, 3021–3024.

van der Woerd, J., F. J. Ryerson, P. Tapponnier, Y. Gaudemer, R. Finkel, A. S. Meriaux, M. Caffee, G. Zhao, and Q. He (1998), Holocene left-slip rate determined by cosmogenic surface dating on the Xidatan segment of the Kunlun fault (Qinghai, China), *Geology*, *26*, 695–698.

van Ngoc, P., D. Boyer, P. Therme, X. Cheng Yuan, L. Li, and G. Yuan Jin (1986), Partial melting zones in the crust in southern Tibet from magnetotelluric results, *Nature*, *319*, 310.

Vergne, J., G. Wittlinger, Q. Hui, P. Tapponnier, G. Poupinet, J. Mei, G. Herquel, and A. Paul (2002), Seismic evidence for stepwise thickening of the crust across the NE Tibetan Plateau, *Earth Planet. Sci. Lett.*, *203*, 25–33.

Wang, Q., et al. (2001), Present-day crustal deformation in China constrained by Global Positioning System measurements, *Science*, *294*, 574–577.

Wannamaker, P. E., G. W. Hohmann, and S. Ward (1984), Magnetotelluric responses of three-dimensional bodies in layered earths, *Geophysics*, *49*, 1517–1533.

Wei, W., et al. (2001), Detection of widespread fluids in the Tibetan crust by magnetotelluric studies, *Science*, *292*, 716–718.

Willett, S. D., and C. Beaumont (1994), Subduction of Asian lithospheric mantle beneath Tibet inferred from models of continental collision, *Nature*, *369*, 642–645.

Wittlinger, G., F. Masson, G. Poupinet, P. Tapponnier, G. Hequel, J. Guilbert, U. Achauer, X. Guanqi, and S. Danian (1996), Seismic tomography of northern Tibet and Kunlun: Evidence for crustal blocks and mantle velocity contrasts, *Earth Planet. Sci. Lett.*, *139*, 263–279.

Yin, A., and T. M. Harrison (2000), Geologic evolution of the Himalayan-Tibetan Orogen, *Annu. Rev. Earth Planet. Sci.*, *28*, 211–280.

Zhao, W., and W. J. Morgan (1987), Injection of Indian crust into Tibetan crust: A two-dimensional finite element model study, *Tectonics*, *6*, 489–504.

Zhao, W., K. D. Nelson and Project INDEPTH team (1993), Deep seismic reflection evidence for continental underthrusting beneath southern Tibet, *Nature*, *366*, 557–559.

Zhu, L., and D. V. Helmberger (1998), Moho offset across the Northern margin of the Tibetan Plateau, *Science*, *281*, 1170–1172.

P. Bedrosian, J. Booker, and S. Li, Department of Earth and Space Sciences, University of Washington, Box 351310, Seattle, WA 98195-1310, USA. (bedros@geophys.washington.edu; booker@geophys.washington.edu; shenghui@apl.washington.edu)

M. Deng, S. Jin, H. Tan, and W. Wei, Department of Applied Geophysics, China University of Geosciences, 29 Xueyuan Road, Beijing, China. (thd@cugb.edu.cn)

A. Jones, Geological Survey of Canada, 615 Booth Street, Ottawa, Ontario, Canada K1A 0E9. (jones@cg.nrcan.gc.ca)

M. Unsworth, Department of Physics, University of Alberta, Edmonton, Canada T6G 2JI. (unsworth@phys.ualberta.ca)